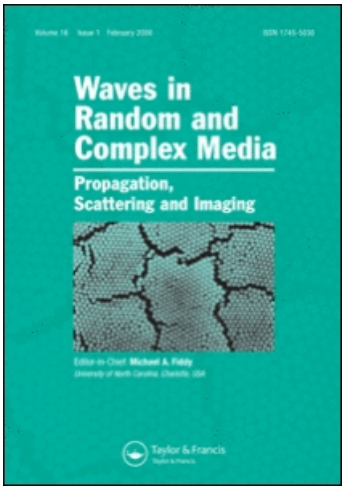

Waves in Random and Complex Media
Publication details, including instructions for authors and subscription information:
http://www.informaworld.com/smpp/title~content=t716100762

A versatile composite surface model for electromagnetic backscattering from seas

Min Zhang[a]; Ding Nie[a]; Hong-Cheng Yin[b]
[a] School of Science, Xidian University, Xi'an, China [b] National Electromagnetic Scattering Laboratory, Beijing, China

First published on: 10 March 2011

To cite this Article Zhang, Min , Nie, Ding and Yin, Hong-Cheng(2011) 'A versatile composite surface model for electromagnetic backscattering from seas', Waves in Random and Complex Media, 21: 2, 348 — 361, First published on: 10 March 2011 (iFirst)
To link to this Article: DOI: 10.1080/17455030.2011.556681
URL: http://dx.doi.org/10.1080/17455030.2011.556681

Waves in Random and Complex Media
Vol. 21, No. 2, May 2011, 348–361

A versatile composite surface model for electromagnetic backscattering from seas

Min Zhang[a]*, Ding Nie[a] and Hong-Cheng Yin[b]

[a]*School of Science, Xidian University, Xi'an, China;* [b]*National Electromagnetic Scattering Laboratory, Beijing, China*

(*Received 17 July 2010; final version received 17 January 2011*)

A versatile composite surface model (VCSM) is presented for estimation of the electromagnetic backscattering coefficient of the sea. Taking into account the statistical characteristics of the sea surface and the validity conditions of component models for the small-scale and large-scale surfaces in the composite surface model (CSM), a method for the two-scale decomposition of sea surfaces is introduced. On this basis, the cutoff wavenumber with wind speed dependence and incident wave frequency dependence is applied to separate the sea spectrum into large- and small-scale components at different sea states with increased accuracy. Then, numerical results of the backscattering coefficient are evaluated and discussed in the case of different wind speeds, polarizations as well as incident frequencies. Finally, the VCSM is verified through the comparisons with the available experimental data, and the comparisons of the VCSM results and the classical CSM results also show that the VCSM behaves better.

1. Introduction

Electromagnetic scattering from a randomly rough surface has been of considerable interest for extensive applications in many fields such as oceanic surveillance, satelliteborne and airborne remote sensing in a marine environment [1,2] and so on. Prediction of ocean electromagnetic scattering characteristics has been developed mainly through the application of different kinds of approaches, for instance, the Kirchhoff approximation (KA) [3], the small perturbation method (SPM) [4], the integral equation method (IEM) [5], the small slope approximation (SSA) [6], the boundary perturbation method (BPM) [7] and the two-scale model (TSM) [8,9]. One of the most frequently employed approaches among them is TSM, which is a composite surface model (CSM) based on the assumption that the sea is composed of larg-scale gravity waves and small-scale capillary ripples. Therefore, the sea surface is simplified to be a rough surface with only two kinds of roughness scales; in addition, small-scale facets are locally tilted by the slope distribution of large-scale facets.

*Corresponding author. Email: mzhang@mail.xidian.edu.cn

ISSN 1745–5030 print/ISSN 1745–5049 online

DOI: 10.1080/17455030.2011.556681
http://www.informaworld.com

In order to describe the scattering characteristics from sea surface accurately, great effort has been dedicated to the modification of the CSM.

In the 1970s, Wu and Fung [10] indicated that the effect of the small irregularities on the scattering characteristics of the large undulations in TSM should be included by modifying the Fresnel reflection coefficients, and verified the advantage of composite theory over single surface theory. Valenzuela [8] reviewed the analytical methods in electromagnetic scattering theory for remote sensing of the ocean, including the CSM. Brown [11] presented an analytical approach to the problem of scattering by composite Gaussian-distributed random surfaces, and discussed the problem of choosing spectral division point between large-scale scattering and small-scale diffraction. Johnson et al. [12] developed a CSM for ocean scattering and applied it in a study of backscattering from a perfectly conducting one-dimensional and two-dimensional Pierson–Moskowitz ocean surfaces. Khenchaf et al. [13,14] studied the regions of validity of the KA and SPM in the bistatic case and extended TSM scattering coefficient computation to the bistatic and cross-polarized condition. Lemaire et al. [15] presented the BPM for composite rough surface scattering, especially ocean-like surface scattering, and then compared the results with IEM. More recently, Awada et al. [16] compared the normalized radar cross-section of an anisotropic ocean surface in a fully bistatic configuration between the TSM and the first-order SSA (SSA-1). Arnold-Bos et al. [17] employed a semi-deterministic TSM to evaluate the sea surface scattering characteristics, so as to be able to incorporate the presence of the ship wakes. Soriano et al. [18] replaced SPM with the SSA-1 to treat the small-scale roughness in the classical TSM. They employed this improved TSM to estimate electromagnetic scattering from sea surfaces.

For the CSM, a cutoff wavenumber is required to divide the sea spectrum into large- and small-scale components. Based on the cutoff wavenumber, the contribution of large- and small-scale facets to the scattering is evaluated by the geometrical optics (GO) and the SPM, respectively. Both methods should be valid in its corresponding range of action. However, it is usually intractable to appropriately select the cutoff wavenumber; in most earlier published literatures [11,19,20], most authors just specified it as a frequency-dependent value for all the sea states considered, whereas with the variation of the sea state, the shares of the contribution of the facets with each scale to scattering should change, that is to say, the cutoff wavenumber should be dependent not only on the incident wave frequency, but also on the wind speed which, to our knowledge, has not been properly considered yet. In this study, the effect of the new frequency-dependent as well as wind speed-dependent cutoff wavenumber is taken into consideration, which is the main contribution of our versatile composite surface model (VCSM) and the improvement of the classical CSM. The purpose of our study was to evaluate electromagnetic backscattering from randomly rough seas using VCSM at various sea state conditions.

In this paper, the theoretical formulae of the VCSM for the estimation of the electromagnetic backscattering from seas are developed first. Second, numerical results of the backscattering coefficient of the VCSM are evaluated and discussed in the case of different wind speeds, polarizations as well as incident frequencies. The VCSM is verified through the comparisons of numerical results with the

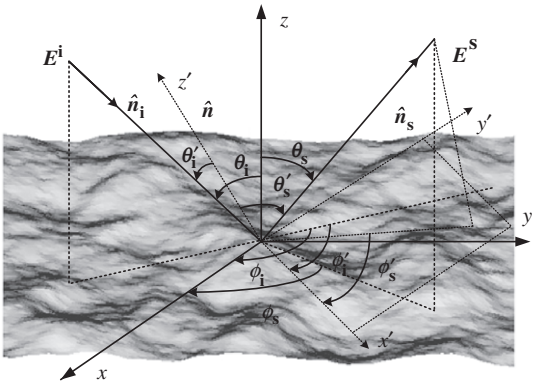

Figure 1. Geometry of the sea surface scattering problem.

experimental data represented by CMOD2-I3 and SASS-II empirical models, and the comparison of the VCSM results and the classical CSM results is also made. Finally, the conclusion of the paper is presented.

2. Electromagnetic scattering from sea surface

The VCSM states that the scattering from such multiscale surface as sea surface can be divided into two components: specular component and diffuse component. The former is caused by large-scale surface components tilted in a way that electromagnetic wave will "bounce" on them according to the law of reflection, for which the GO is applied. The latter is caused by the Bragg process of small-scale components locally tilted by large-scale ones, for which the averaged SPM is used. The VCSM result is indeed a sum of the GO result and a weighted average of the local SPM result, the weight being related to the probability distribution of the surface slopes. The geometry of the sea surface scattering problem is shown in Figure 1.

2.1. *Computation of specular scattering component*

Considering incident plane waves $\boldsymbol{E}^{\mathrm{i}} = \hat{\boldsymbol{a}} E_0 e^{-jk\hat{\boldsymbol{n}}_{\mathrm{i}}\cdot\hat{\boldsymbol{r}}}$ impinge on a two-dimensional rough sea surface, $z(x, y)$ represents the roughness elevation function of the point $(x, y) \in$ sea surface S, Based on GO, the scattered field of a dielectric rough sea surface is expressed as [21]

$$\boldsymbol{E}^{\mathrm{s}} = \frac{-jke^{-jkR_0}}{4\pi R_0}\hat{\boldsymbol{n}}_{\mathrm{s}} \times \int_S [\hat{\boldsymbol{n}} \times \boldsymbol{E} - \eta\hat{\boldsymbol{n}}_{\mathrm{s}} \times (\hat{\boldsymbol{n}} \times \boldsymbol{H})]e^{jk(\hat{\boldsymbol{n}}_{\mathrm{s}}-\hat{\boldsymbol{n}}_{\mathrm{i}})\cdot\boldsymbol{r}}\mathrm{d}S, \tag{1}$$

where $\hat{\boldsymbol{a}}$ is the unit polarization vector, $\hat{\boldsymbol{n}}_{\mathrm{s}}$ and $\hat{\boldsymbol{n}}_{\mathrm{i}}$ represent unit vectors in the scattered direction and incident direction, respectively, $\hat{\boldsymbol{n}}$ denotes the unit vector normal to the sea surface $z(x, y)$, and k is the incident field wavenumber. η is the intrinsic impedance of the sea surface. $\boldsymbol{E}$ and $\boldsymbol{H}$ are the total electric and magnetic

fields on the sea surface. This approach assumes that scattering can occur only along directions for which there are specular points on the surface, the effects of local diffraction and multiple scattering are excluded. Hence, the phase term of Equation (1) can be expressed as

$$\psi = jk(\hat{\boldsymbol{n}}_{\mathrm{s}} - \hat{\boldsymbol{n}}_{\mathrm{i}}) \cdot \boldsymbol{r} = k_{\mathrm{r}x}x + k_{\mathrm{r}y}y + k_{\mathrm{r}z}z \tag{2}$$

where

$$\hat{\boldsymbol{n}}_{\mathrm{i}} = \hat{x}\sin\theta_{\mathrm{i}}\cos\phi_{\mathrm{i}} + \hat{\boldsymbol{y}}\sin\theta_{\mathrm{i}}\sin\phi_{\mathrm{i}} - \hat{z}\cos\theta_{\mathrm{i}} \tag{3}$$

$$\hat{\boldsymbol{n}}_{\mathrm{s}} = \hat{\boldsymbol{x}}\sin\theta_{\mathrm{s}}\cos\phi_{\mathrm{s}} + \hat{\boldsymbol{y}}\sin\theta_{\mathrm{s}}\sin\phi_{\mathrm{s}} + \hat{\boldsymbol{z}}\cos\theta_{\mathrm{s}} \tag{4}$$

$$\hat{\boldsymbol{n}} = (-\hat{\boldsymbol{x}}\gamma_x - \hat{\boldsymbol{y}}\gamma_y + \hat{\boldsymbol{z}})/(1 + \gamma_x^2 + \gamma_y^2)^{1/2} \tag{5}$$

$$k_{\mathrm{r}x} = k(\sin\theta_{\mathrm{s}}\sin\phi_{\mathrm{s}} - \sin\theta_{\mathrm{i}}\sin\phi_{\mathrm{i}}) \tag{6}$$

$$k_{\mathrm{r}y} = k(\sin\theta_{\mathrm{s}}\sin\phi_{\mathrm{s}} - \sin\theta_{\mathrm{i}}\sin\phi_{\mathrm{i}}) \tag{7}$$

$$k_{\mathrm{r}z} = k(\cos\theta_{\mathrm{s}} + \cos\theta_{\mathrm{i}}) \tag{8}$$

$$k_{\mathrm{r}} = (k_{\mathrm{r}x}^2 + k_{\mathrm{r}y}^2 + k_{\mathrm{r}z}^2)^{1/2}. \tag{9}$$

$(\theta_{\mathrm{i}}, \theta_{\mathrm{s}}, \phi_{\mathrm{i}}, \phi_{\mathrm{s}})$ are the configuration angles, which denote incident angle, scattering angle, azimuth angle of incident wave and azimuth angle of scattered wave, respectively. γ_x and γ_y denote sea surface slopes along x- and y-directions, respectively. To determine the stationary phase point, we differentiate Equation (2) with respect to x and y, and set it equal to zero, then we have

$$\gamma_x = -\frac{k_{\mathrm{r}x}}{k_{\mathrm{r}z}}, \quad \gamma_y = -\frac{k_{\mathrm{r}y}}{k_{\mathrm{r}z}}. \tag{10}$$

After applying the stationary-phase approximation [22] to simplify the corresponding scattered field formula, the polarized backscattering coefficient developed by GO can be given as

$$\sigma_{\alpha\beta,\mathrm{GO}} = \frac{\pi k^2 k_{\mathrm{r}}^2}{k_{\mathrm{r}z}} \left|U_{\alpha\beta}\right|^2 P(\gamma_x, \gamma_y) \tag{11}$$

where $\alpha, \beta = \mathrm{H}$ or V, α represents polarization condition of the scattered waves, β denotes the counterpart of the incident waves, H indicates horizontal polarization, V vertical polarization. $U_{\alpha\beta}$ is a polarimetic parameter depending on the configuration angles $(\theta_{\mathrm{i}}, \theta_{\mathrm{s}}, \phi_{\mathrm{i}}, \phi_{\mathrm{s}})$ and on Fresnel coefficients [21].

$$U_{\mathrm{HH}} = \frac{k_{\mathrm{r}}|k_{\mathrm{r}z}|[R_{\mathrm{V}}(\hat{\boldsymbol{h}}_{\mathrm{s}} \cdot \hat{\boldsymbol{n}}_{\mathrm{i}})(\hat{\boldsymbol{h}}_{\mathrm{i}} \cdot \hat{\boldsymbol{n}}_{\mathrm{s}}) + R_{\mathrm{H}}(\hat{\boldsymbol{v}}_{\mathrm{s}} \cdot \hat{\boldsymbol{n}}_{\mathrm{i}})(\hat{\boldsymbol{v}}_{\mathrm{i}} \cdot \hat{\boldsymbol{n}}_{\mathrm{s}})]}{[(\hat{\boldsymbol{h}}_{\mathrm{s}} \cdot \hat{\boldsymbol{n}}_{\mathrm{i}})^2 + (\hat{\boldsymbol{v}}_{\mathrm{s}} \cdot \hat{\boldsymbol{n}}_{\mathrm{i}})^2]kk_{\mathrm{r}z}} \tag{12}$$

$$U_{\mathrm{VV}} = \frac{k_{\mathrm{r}}|k_{\mathrm{r}z}|[R_{\mathrm{H}}(\hat{\boldsymbol{h}}_{\mathrm{s}} \cdot \hat{\boldsymbol{n}}_{\mathrm{i}})(\hat{\boldsymbol{h}}_{\mathrm{i}} \cdot \hat{\boldsymbol{n}}_{\mathrm{s}}) + R_{\mathrm{V}}(\hat{\boldsymbol{v}}_{\mathrm{s}} \cdot \hat{\boldsymbol{n}}_{\mathrm{i}})(\hat{\boldsymbol{v}}_{\mathrm{i}} \cdot \hat{\boldsymbol{n}}_{\mathrm{s}})]}{[(\hat{\boldsymbol{h}}_{\mathrm{s}} \cdot \hat{\boldsymbol{n}}_{\mathrm{i}})^2 + (\hat{\boldsymbol{v}}_{\mathrm{s}} \cdot \hat{\boldsymbol{n}}_{\mathrm{i}})^2]kk_{\mathrm{r}z}} \tag{13}$$

where R_H and R_V are the Fresnel reflection coefficients for horizontal polarization and vertical polarization, respectively, $\hat{\boldsymbol{h}}_i$ and $\hat{\boldsymbol{v}}_i$ are unit polarization vectors for incident horizontal and vertical waves, $\hat{\boldsymbol{h}}_s$ and $\hat{\boldsymbol{v}}_s$ are unit polarization vectors for scattered horizontal and vertical waves, which can be tracked in [21]. $P(\gamma_x, \gamma_y)$ is the probability density function (PDF) of the surface slopes, here, the improved form of the PDF by Cox and Munk [23] is applied in our model, and its explicit expression will be given later in Equation (22).

2.2. *Computation of diffuse scattering component*

The diffuse component of the scattering is numerically evaluated by SPM. As in the VCSM, the small-scale facets ride on the large-scale surfaces, the modulation effect of the large-scale waves should be taken into account by averaging the backscattering coefficient of small-scale waves over the distribution of the large-scale waves, which can be expressed as [9]

$$\sigma_{\alpha\beta,\mathrm{SPM}} = \int_{-\infty}^{\infty}\int_{-ctg\theta_i}^{\infty} \sigma^0_{\alpha\beta,\mathrm{SPM}}(\theta_i')(1+\gamma_x tg\theta_i)\, P(\gamma_x', \gamma_y')\, \mathrm{d}\gamma_x\, \mathrm{d}\gamma_y, \tag{14}$$

where γ_x and γ_y represent sea surface slopes along x- and y-directions, respectively. Equation (14) just denotes the SPM that averaged by the geometric tilting effect caused by small-scale surfaces "ride" on the large-scale ones. Let the unprimed coordinates be the reference frame and the primed coordinates be the local frame, see in Figure 1, so θ_i' denotes the local incident angle, which is defined as

$$\cos\theta_i' = -(\hat{\boldsymbol{n}}\cdot\hat{\boldsymbol{n}}_i) = (\cos\theta_i + \gamma_x \sin\theta_i \cos\phi_i + \gamma_y \sin\theta_i \sin\phi_i)/(1+\gamma_x^2+\gamma_y^2)^{1/2}. \tag{15}$$

$\sigma^0_{\alpha\beta,\mathrm{SPM}}$ is the scattering coefficient of the small-scale sea surface

$$\sigma^0_{\alpha\beta,\mathrm{SPM}}(\theta_i') = 8k^4\cos^4\theta_i' \left|\chi_{\alpha\beta}\right|^2 W(K,\varphi)/K \tag{16}$$

where $\chi_{\alpha\beta}$ is the polarization coefficient reported in [9],

$$\chi_{\mathrm{HH}} = -\frac{(\varepsilon_r - 1)\cos\phi_s}{[\cos\theta_i + (\varepsilon_r - \sin^2\theta_i)^{1/2}][\cos\theta_s + (\varepsilon_r - \sin^2\theta_s)^{1/2}]} \tag{17}$$

$$\chi_{\mathrm{VV}} = \frac{(\varepsilon_r - 1)[\varepsilon_r \sin\theta_i \sin\theta_s - \cos\phi_s(\varepsilon_r - \sin^2\theta_i)^{1/2}(\varepsilon_r - \sin^2\theta_s)^{1/2}]}{[\varepsilon_r \cos\theta_i + (\varepsilon_r - \sin^2\theta_i)^{1/2}][\varepsilon_r \cos\theta_s + (\varepsilon_r - \sin^2\theta_s)^{1/2}]} \tag{18}$$

ε_r denotes the permittivity of the sea water. $K = 2k\sin\theta_i'$, $W(K,\varphi)$ represents the two-dimensional sea spectrum for small-scale surface and can be expressed as

$$W(K,\varphi) = \begin{cases} S(K,\varphi), & K \geq k_c \\ 0, & K < k_c \end{cases}, \tag{19}$$

$S(K,\varphi) = S(K)\Phi(K,\varphi)$, $S(K)$ is the omnidirectional sea spectrum [24], $\Phi(K,\varphi)$ the angular spreading function [24], and k_c the cutoff wavenumber.

The slope probability density function of sea surface proposed by Cox and Munk is often exploited for the calculation of Equation (14), which can be written as

$$P(\gamma'_x, \gamma'_y) = \frac{F(\gamma'_x, \gamma'_y)}{2\pi s_{\mathrm{u}} s_{\mathrm{c}}} \exp\left[-\frac{\gamma'^2_x}{2s_{\mathrm{u}}^2} - \frac{\gamma'^2_y}{2s_{\mathrm{c}}^2}\right] \tag{20}$$

where $F(\gamma'_x, \gamma'_y)$, γ'_x and γ'_y are reported in [9]. s_{u}^2 and s_{c}^2 are the slope variances of the sea surface in the upwind direction and crosswind direction, respectively. The Cox and Munk's model is for the sea surface, both large scale and small scale, whereas the VCSM only needs the slope distribution of the large-scale surface. It is of great necessity to remove contributions to s_{u}^2 and s_{c}^2 from the small-scale surfaces, thus, we have the slope variances of the large-scale-only sea surface in the upwind direction and crosswind direction, s_{ul} and s_{cl}:

$$\begin{cases} s_{\mathrm{ul}}^2 = \int_0^{k_{\mathrm{c}}} \mathrm{d}\kappa \int_0^{2\pi} (\kappa \cos\varphi)^2 S(\kappa, \varphi) \mathrm{d}\varphi \\ s_{\mathrm{cl}}^2 = \int_0^{k_{\mathrm{c}}} \mathrm{d}\kappa \int_0^{2\pi} (\kappa \sin\varphi)^2 S(\kappa, \varphi) \mathrm{d}\varphi. \end{cases} \tag{21}$$

The final form of the slope probability density function would be used in our VCSM is denoted as:

$$P(\gamma'_x, \gamma'_y) = \frac{F(\gamma'_x, \gamma'_y)}{2\pi s_{\mathrm{ul}} s_{\mathrm{cl}}} \exp\left[-\frac{\gamma'^2_x}{2s_{\mathrm{ul}}^2} - \frac{\gamma'^2_y}{2s_{\mathrm{cl}}^2}\right]. \tag{22}$$

Moreover, for large incident angle, the incidence and scattering shadowing effect of the sea surface are strong, the monostatic shadowing function $S(v_1)$ developed by Bourlier et al. [25] is utilized to account for the shadowing effect in this paper.

In the end, based on Equation (11) and Equation (14), the backscattering coefficient for an anisotropic rough sea surface is given by the VCSM [26]

$$\begin{aligned} \sigma_{\alpha\beta} = {} & \frac{\pi k^2 k_{\mathrm{r}}^2}{k_{\mathrm{r}z}^4} \left|U_{\alpha\beta}\right|^2 P(\gamma_x, \gamma_y) \\ & + S(v_1) \int_{-\infty}^{\infty} \int_{-ctg\theta_{\mathrm{i}}}^{\infty} \sigma^0_{\alpha\beta,\mathrm{SPM}}(\theta'_{\mathrm{i}})(1 + \gamma_x tg\theta_{\mathrm{i}})\, P(\gamma'_x, \gamma'_y)\, \mathrm{d}\gamma_x \mathrm{d}\gamma_y. \end{aligned} \tag{23}$$

2.3. *Determination of cutoff wavenumber*

In the above section, we presented the electromagnetic component models of the VCSM for scattering from seas with large-scale surface components and small-scale surface components. Different constraints would imposed on each scale for the application of GO and SPM. In previous studies, the cutoff wavenumber k_{c} has been chosen differently for various authors ranging from $k/1.5$ to $k/40$ [27], which is specified as a frequency-dependent value for all the sea states. Whereas at different sea state conditions, the shares of the contribution to total scattering from large-scale and small-scale sea surface should change, that is to say, the k_{c} should be incident frequency-dependent and wind speed-dependent according to various sea states, which is also in a logical sense. Thus, both the sea surface statistical characteristics

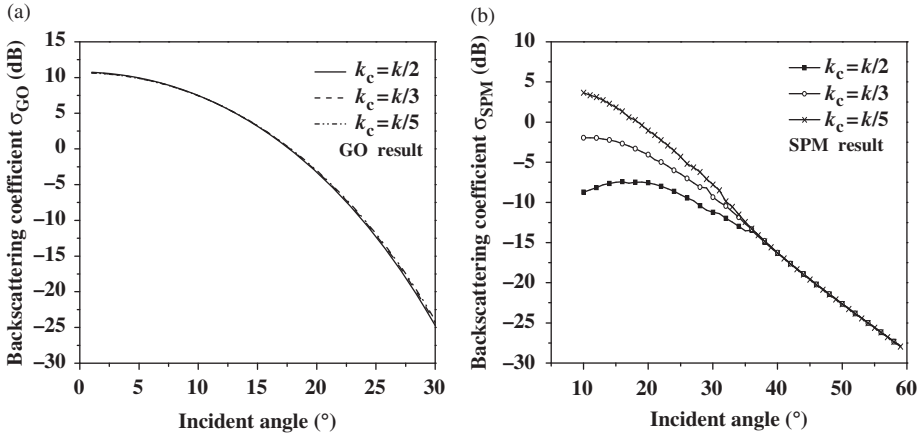

Figure 2. The influence of the cutoff wavenumber k_c on the GO model and the SPM: (a) GO; (b) SPM.

and the validity conditions of scattering models for the small-scale surface and the large-scale surface are introduced to evaluate the proper k_c.

From the Equation (23), it can be found that the final backscattering coefficient is composed of two components: σ_{GO} and σ_{SPM}. The influences of the cutoff wavenumber k_c on the two model (GO and SPM) are depicted in Figure 2. From this figure, it is clearly shown that the influence of k_c on GO model is small in both the small angle region and the transition region, which can be ignored, while the σ_{SPM} is sensitive to the variation of the k_c for incident angles in the vicinity of the transition region, but for larger incident angles ($30^\circ - 60^\circ$), the σ_{SPM} changes little for different k_c. From this point, it can be concluded that the choice of different k_c would affect the final backscattering coefficient greatly in the vicinity of the transition region, while in the near specular region or in the middle-to-large angle region, this kind of influence is relatively small, or even could be neglected. Based on the above viewpoints, equating the criterions associated with the GO and the SPM is chosen for calculating the proper k_c for all the specified incident angles we are interested in.

The validity conditions of the scattering models for the small- and large-scale surfaces are given, respectively [11,14]

$$4k^2\zeta_s^2\cos^2\theta_i \ll 1. \tag{24}$$

$$\lambda\xi_c\cos^3\theta_i \ll 1, \quad k\zeta_l > \sqrt{10}/|\cos\theta_s + \cos\theta_i| \tag{25}$$

where ζ_s and ζ_l are the root-mean-square height of small-scale surface and large-scale surface, respectively,

$$\begin{cases} \zeta_l^2 = \int_0^{k_c} S(\kappa)\mathrm{d}\kappa \\ \zeta_s^2 = \int_{k_c}^{\infty} S(\kappa)\mathrm{d}\kappa \end{cases}. \tag{26}$$

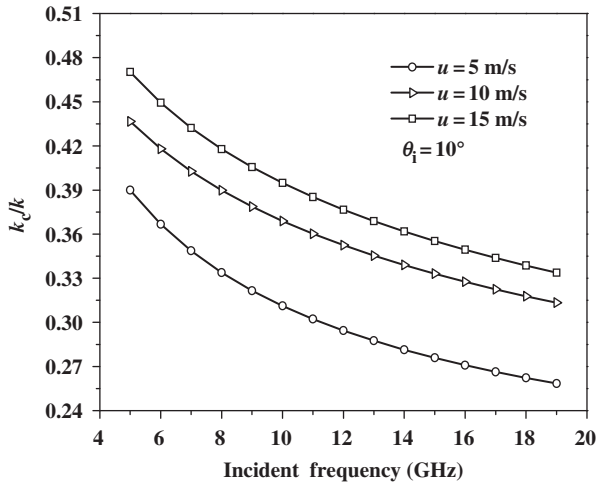

Figure 3. The parameter k_c/k versus incident frequency for different wind speeds.

λ denotes the wavelength of incident electromagnetic wave. ξ_c is the standard deviation of the sea surface mean curvature. It can be expressed as follows:

$$\xi_c^2 = \int_0^{k_c} \kappa^4 S(\kappa) \mathrm{d}\kappa. \tag{27}$$

Last but not least, letting Equation (24) and the first part of Equation (25) have the same limit value, we have

$$4k^2 \cos^2 \theta_i \int_{k_c}^{\infty} S(\kappa) \mathrm{d}\kappa = \lambda \cos^3 \theta_i \sqrt{\int_0^{k_c} \kappa^4 S(\kappa) \mathrm{d}\kappa}. \tag{28}$$

Applying Equation (28), we can find the cutoff wavenumber k_c.

3. Numerical results and discussion

To investigate the performance of the proposed model, the numerical results of backscattering coefficient using the VCSM developed in this study are given and discussed in this section.

Figure 3 shows the dependence of the parameter k_c/k on the incident frequency in the case of different wind speeds u. The incident angle is 10°. It is observed that as the incident frequency rise, k_c/k decreases gradually at a gentle rate at the beginning and then descends at a much lower rate. It is also not difficult to observe that k_c/k varies in a similar pattern for different wind speeds ranged from 5 m/s to 15 m/s. When the wind speed increases, the value of k_c/k for the fixed incident frequency rises accordingly. This is consistent with the result of Lemaire et al. [15].

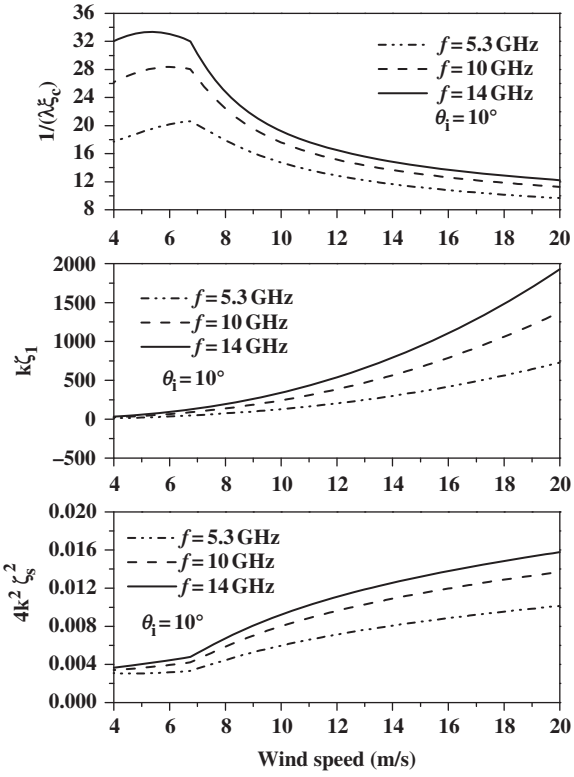

Figure 4. The parameters $4k^2\zeta_s^2$, $k\zeta_l$ and $1/(\lambda\xi_c)$ versus the wind speed for different incident frequencies.

To check whether the validity conditions in the Equations (24) and (25) are satisfied or not, the dependence of the parameters $4k^2\zeta_s^2$, $k\zeta_l$ and $1/(\lambda\xi_c)$ on the wind speed with respect to different incident frequencies is depicted in Figure 4. The incident angle equals to 10°. First, when the wind speed changes gradually from 4 m/s to 20 m/s, it can be seen that the value of $4k^2\zeta_s^2$ is always far less than 1 with respect to the three fixed incident frequencies, and $\cos^2\theta_i$ has its maximum of 1 at $\theta_i = 0°$. Thus, Equation (24) is satisfied. Second, in backscattering configuration, the larger the θ_i is, the greater the value of $\sqrt{10}/|\cos\theta_s + \cos\theta_i|$ will be. Even if we set θ_i and θ_s to be as great a value as 80°, then $\sqrt{10}/|\cos\theta_s + \cos\theta_i|$ has a value of 9.1054, however, $k\zeta_l$ attains its minimum of 12.8938 at the wind speed of 4 m/s for incident frequency of 5.3 GHz. Finally, the parameter $1/(\lambda\xi_c)$ obtains its minimum of 9.6576 at the wind speed of 20 m/s for incident frequency of 5.3 GHz in this figure. Thus, the Equation (25) is also quite well satisfied. It is implied that the method for the two-scale decomposition of sea surfaces is well justified.

To illustrate the performance of the VCSM with new incident frequency-dependent and wind-dependent k_c presented in the paper, we calculate

the backscattering coefficient with respect to different wind speeds for HH- and VV-polarizations. The electromagnetic incident frequency is chosen as 13.9 GHz in K_u-band. The wind speed at a 10 m altitude above the sea surface is fixed to 5 m/s, 10 m/s and 15 m/s, respectively, the emitter is supposed to be in the upwind direction. The classical CSM results for the popular frequency-dependent-only k_c of $k/2$, $k/3$, $k/4$ as well as $k/5$ and experimental data of SASS-II empirical model [28] are chosen for comparison. For clarity, the relative deviation of the VCSM results and the CSM results from that of SASS-II model ($(\sigma - \sigma_{\text{SASS-II}})/\sigma$) is plotted in Figure 5, which could be denoted as $Y_{\text{rd}} = (\sigma - \sigma_{\text{exp}})/\sigma$.

At the wind speed of 5 m/s, it is clearly shown that the CSM results for the k_c of $k/2$ and $k/3$ have relatively greater deviations from the experimental data, especially for the k_c of $k/2$ case. Among other three curves, the VCSM result and the CSM result for the k_c of $k/4$ behave overall better than that for the k_c of $k/5$. While at the wind speed of 10 m/s, for the HH-polarization case, it can be explicitly observed that the VCSM obtains relatively the least deviation from the experimental data, and the CSM for the k_c of $k/3$ performs better than the CSM for any other three k_c do; for the VV-polarization case, the relatively least derivation from the experimental data is obtained by the VCSM and the CSM result for the k_c of $k/2$. Finally, referring to the case of wind speed of 15 m/s, we can see that the VCSM result is the closest to the experimental data among all five curves.

Moreover, the backscattering coefficient with the incident frequency of 5.3 GHz in C-band is also calculated by the VCSM. To justify the VCSM in C-band, the classical CSM results for the popular frequency-dependent-only k_c of $k/2$, $k/3$, $k/4$ as well as $k/5$ and experimental data represented by CMOD2-I3 model [29] are also presented for comparison. There is VV polarization only for the CMOD2-I3 model, thus numerical results in VV polarization are given here. Like in Figure 5, Y_{rd} is depicted in Figure 6. It is not difficult to find that the VCSM results get closer to the experimental data than that of the CSM for other k_c from an overall point of view, especially at large wind speed and in the GO-SPM transition region ($20^\circ - 30^\circ$).

To further evaluate the performance of different models objectively, the average norm of Y_{rd} (ANY) for Ku-band and C-band are calculated and shown in Table 1 and Table 2, respectively, which can reflect derivation of the model result from the experimental data statistically. One of the four CSM results may be close to the VCSM result or even a little better than the VCSM under certain circumstance, however, none of these four CSM could have more stable good performance than the VCSM. Thus, in view of the overall situation, the VCSM performs better than the CSM with respect to different wind speeds and polarization conditions.

All these show that the proposed method for the two-scale decomposition of the sea surface provides a nice compromise between each scale, and aforementioned comparisons also show that the VCSM we proposed constitutes an improvement compared to models in which k_c/k is set as an arbitrary value. It can be indicated finally that the VCSM is more suitable for sea surface electromagnetic scattering estimation than the traditional CSM.

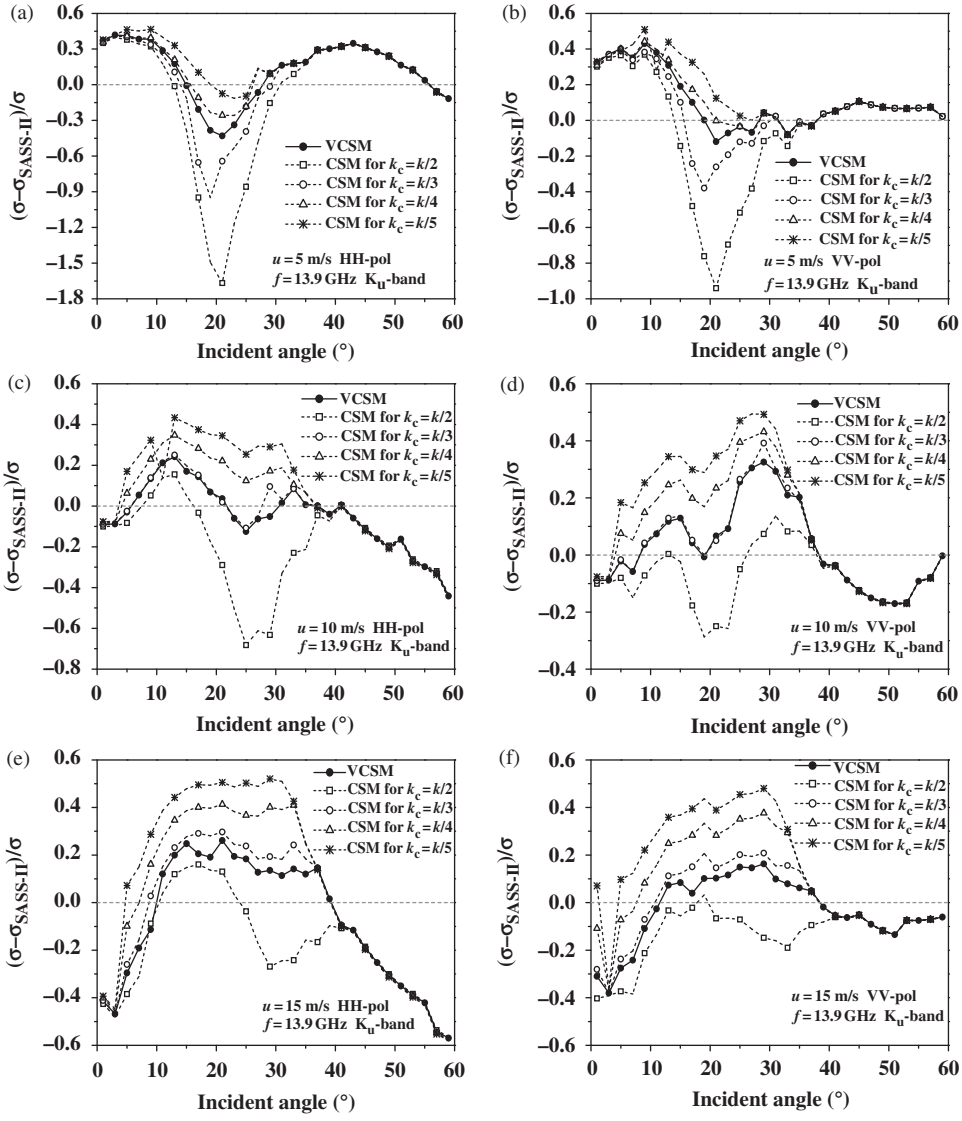

Figure 5. The relative deviation of the VCSM results and the CSM results for various cutoff wavenumbers k_c from that of SASS-II model. Incident frequency: 13.9 GHz (K_u-band). (a, b) $u=5$ m/s, (c, d) $u=10$ m/s, (e, f) $u=15$ m/s.

4. Conclusion

A versatile composite surface model, VCSM, is proposed for sea surface electromagnetic backscattering estimation in this paper. First, we present the detailed deduction of the proposed VCSM for backscattering from composite rough sea surfaces, this model takes statistical characteristics of the sea surface and the validity

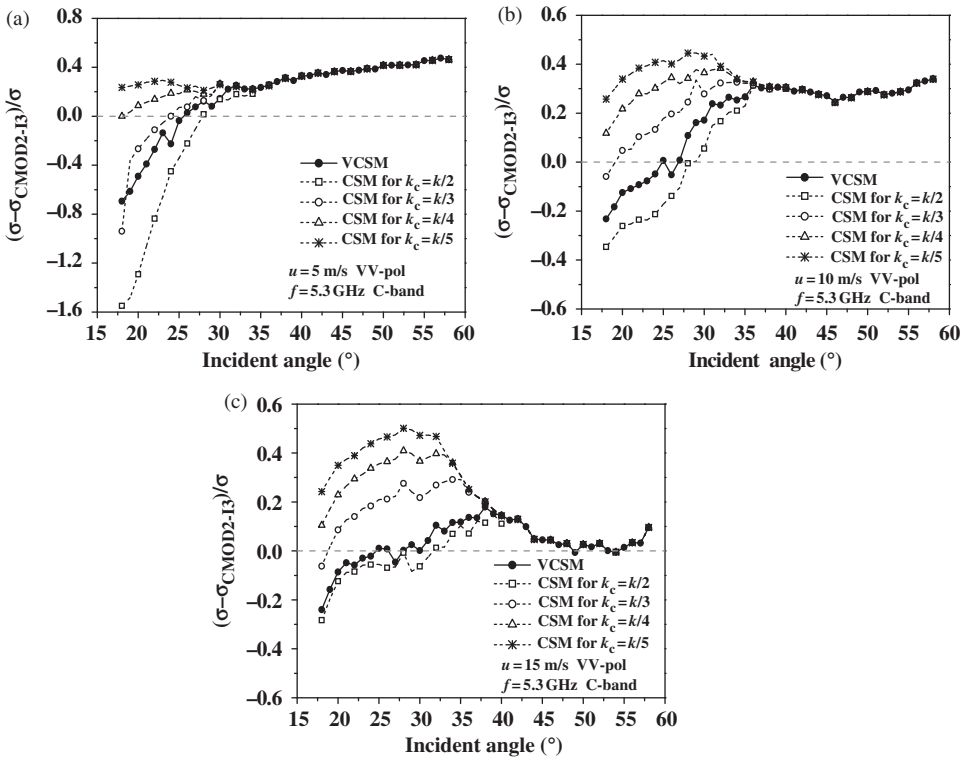

Figure 6. The relative deviation of the VCSM results and the CSM results for other different popular k_c from that of CMOD2-I3 model for the case of VV-polarization. Incident frequency: 5.3 GHz (C-band). (a) $u = 5$ m/s, (b) $u = 10$ m/s, (c) $u = 15$ m/s.

Table 1. The average norm of Y_{rd} (ANY) for VCSM and CSM for different popular k_c in K_u-band.

	$u = 5$ m/s		$u = 10$ m/s		$u = 15$ m/s	
	HH-pol	VV-pol	HH-pol	VV-pol	HH-pol	VV-pol
VCSM	6.3289E−2	3.5644E−2	2.7523E−2	4.3812E−2	4.1750E−2	2.3776E−2
CSM for $k/2$	1.8506E−1	1.0364E−1	8.5463E−2	3.3661E−2	3.9280E−2	2.5613E−2
CSM for $k/3$	1.0181E−1	4.5979E−2	2.8955E−2	4.7022E−2	5.4090E−2	3.6267E−2
CSM for $k/4$	5.4711E−2	3.9210E−2	5.0079E−2	6.6833E−2	8.4325E−2	6.6542E−2
CSM for $k/5$	5.4067E−2	4.9214E−2	6.8689E−2	8.3811E−2	1.0551E−1	8.7869E−2

conditions of scattering models for the small-scale surface and the large-scale surface into account for the cutoff wavenumber, and this crucial consideration to evaluate proper cutoff wavenumber makes the predictions more accurate at different sea state conditions. Furthermore, the dependences of the backscattering coefficient on the incident angle and polarization state are calculated and compared with the

Table 2. The average norm of Y_{rd} (ANY) for VCSM and CSM for different popular k_c in C-band.

	u=5 m/s	u=10 m/s	u=15 m/s
	VV-pol	VV-pol	VV-pol
VCSM	9.2476E−2	3.4512E−2	2.4295E−2
CSM for $k/2$	2.2986E−1	5.7776E−2	3.2502E−2
CSM for $k/3$	8.7246E−2	4.9434E−2	5.0518E−2
CSM for $k/4$	4.5997E−2	8.1302E−2	8.8472E−2
CSM for $k/5$	7.0700E−2	1.0771E−1	1.1664E−1

experimental data, and the comparisons of the VCSM results and the CSM results for k_c/k chosen as some fixed values show that the results of the VCSM fit the experimental data better in both the K_u- and C-bands. Therefore, we conclude that the VCSM proposed in this paper can be a competitive tool for sea surface electromagnetic backscattering estimation. In order to increase more practicability, the bistatic scattering from composite rough sea surface based on the VCSM and its application to remote sensing of various marine environments will be studied in future work.

Acknowledgements

The authors are grateful to the referees for suggesting on the paper, and also thank the National Natural Science Foundation of China under Grant No. 60871070, the National Pre-research Foundation and the Foundation of the National Electromagnetic Scattering Laboratory to support this kind of research.

References

[1] D.E. Barrick, *First-order theory and analysis of MF/HF/VHF scatter from the sea*, IEEE Trans. Antennas Propagat. AP-20 (1972), pp. 2–10.
[2] D.E. Barrick, J.M. Headrick, R.W. Bogle, and D.D. Crombie, *Sea backscatter at HF: Interpretation and utilization of the echo*, IEEE Proc. 62 (1974), pp. 673–680.
[3] J.A. Ogilvy, *Theory of Wave Scattering from Random Rough Surfaces*, Adam Hilger, Bristol, 1991.
[4] G.R. Valenzuela, *Scattering of electromagnetic waves from a tilted slightly rough surfaces*, Radio Sci. 3 (1968), pp. 1057–1066.
[5] A.K. Fung, Z. Li, and K.S. Chen, *Backscattering from a randomly rough dielectric surface*, IEEE Trans. Geosci. Remote Sens. 30 (1992), pp. 356–369.
[6] A.G. Voronovich, *Small-slope approximation for electromagnetic wave scattering at a rough interface of two dielectric half-spaces*, Waves Random Complex Media 4 (1994), pp. 337–367.
[7] A. Guissard, P. Sobieski, and C. Baufays, *A unified approach to bistatic scattering for active and passive remote sensing of rough ocean surfaces*, Trends Geophys. Res. 1 (1992), pp. 43–68.
[8] G.R. Valenzuela, *Theories for the interaction of electromagnetic and oceanic waves – a review*, Bound. Layer Met. 13 (1978), pp. 61–85.
[9] H.L. Chan and A.K. Fung, *A theory of sea scatter at large incident angles*, J. Geophys. Res. 82 (1997), pp. 3439–3444.

[10] S.T. Wu and A.K. Fung, *A noncoherent model for microwave emissions and backscattering from the sea surface*, J. Geophys. Res. 77 (1972), pp. 5917–5929.
[11] G.S. Brown, *Backscattering from a Gaussian-distributed perfectly conducting rough surface*, IEEE Trans. Antennas Propagat. AP-26 (1978), pp. 472–482.
[12] J.T. Johnson, R.T. Shin, J.A. Kong, L. Tsang, and K. Pak, *A numerical study of the composite surface model for ocean backscattering*, IEEE Trans. Geosci. Remote Sens. 36 (1998), pp. 72–83.
[13] A. Khenchaf and O. Airiau, *Bistatic radar moving returns from sea surface*, IEICE Trans. Electron. E83-C (2000), pp. 1827–1835.
[14] Khenchaf, *Bistatic scattering and depolarization by randomly rough surfaces: Application to the natural rough surfaces in X-band*, Waves Random Complex Media 11 (2001), pp. 61–89.
[15] D. Lemaire, P. Sobieski, C. Craeye, and A. Guissard, *Two-scale models for rough surface scattering: comparison between the boundary perturbation method and the integral equation method*, Radio Sci. 37 (2002), pp. 1–16.
[16] A. Awada, M.Y. Ayari, A. Khenchaf, and A. Coatanhay, *Bistatic scattering from an anisotropic sea surface: Numerical comparison between the first-order SSA and the TSM models*, Waves Random Complex Media 16 (2006), pp. 383–394.
[17] A. Arnold-Bos, A. Khenchaf, and A. Martin, *Bistatic radar imaging of the marine environment – Part I: Theoretical background*, IEEE Trans. Geosci. Remote Sens. 45 (2007), pp. 3372–3383.
[18] G. Soriano and C.-A. Guerin, *A cutoff invariant two-scale model in electromagnetic scattering from sea surfaces*, IEEE Geosci. Remote Sens. Lett. 5 (2008), pp. 199–203.
[19] W.J. Plant, *Two-scale model for short wind-generated waves and scatterometry*, J. Geophys. Res. 91 (1986), pp. 10735–10749.
[20] D.R. Thompson, *Calculation of radar backscatter modulations from internal waves*, J. Geophys. Res. 93 (1988), pp. 12371–12380.
[21] F.T. Ulaby, R.K. Moore, and A.K. Fung, *Microwave Remote Sensing: Active and Passive*, Vol. 2, Addison-Wesley Publishing, London, 1982.
[22] D.E. Barrick, *Rough surface scattering based on the specular point theory*, IEEE Trans. Antennas Propagat. AP-16 (1968), pp. 449–454.
[23] C. Cox and W. Munk, *Measurement of the roughness of the sea surface from photographs of the sun's glitter*, J. Opt. Soc. Am. 44 (1954), pp. 838–850.
[24] T. Elfouhaily, B. Chapron, K. Katsaros, and D. Vandemark, *A unified directional spectrum for long and short wind-driven waves*, J. Geophys. Res. 102 (1997), pp. 15781–15796.
[25] C. Bourlier, G. Berginc, and J. Saillard, *One and two-dimensional shadowing functions for any height and slope stationary uncorrelated surface in the monostatic and bistatic configurations*, IEEE Trans. Antennas Propagat. 50 (2002), pp. 312–324.
[26] F.G. Bass and I.M. Fuks, *Wave Scattering from Statistically Rough Surfaces*, Pergamon Press, Oxford, 1979.
[27] A.G. Voronovich and V.U. Zavorotny, *Theoretical model for scattering of radar signals in K_u- and C-bands from a rough sea surface with breaking waves*, Waves Random Media 11 (2001), pp. 247–269.
[28] F.J. Wentz, S. Peteherych, and L.A. Thomas, *A model function for ocean radar cross sections at 14.6 GHz*, J. Geophys. Res. 89 (1984), pp. 3689–3704.
[29] A. Bentamy, P. Queffeulou, Y. Quilfen, and K. Katsaros, *Ocean surface wind fields estimated from satellite active and passive microwave instruments*, IEEE Trans. Geosci. Remote Sens. 37 (1999), pp. 2469–2486.